

INFORMATION TO USERS

This manuscript has been reproduced from the microfilm master. UMI films the text directly from the original or copy submitted. Thus, some thesis and dissertation copies are in typewriter face, while others may be from any type of computer printer.

The quality of this reproduction is dependent upon the quality of the copy submitted. Broken or indistinct print, colored or poor quality illustrations and photographs, print bleedthrough, substandard margins, and improper alignment can adversely affect reproduction.

In the unlikely event that the author did not send UMI a complete manuscript and there are missing pages, these will be noted. Also, if unauthorized copyright material had to be removed, a note will indicate the deletion.

Oversize materials (e.g., maps, drawings, charts) are reproduced by sectioning the original, beginning at the upper left-hand corner and continuing from left to right in equal sections with small overlaps. Each original is also photographed in one exposure and is included in reduced form at the back of the book.

Photographs included in the original manuscript have been reproduced xerographically in this copy. Higher quality 6" x 9" black and white photographic prints are available for any photographs or illustrations appearing in this copy for an additional charge. Contact UMI directly to order.



University Microfilms International
A Bell & Howell Information Company
300 North Zeeb Road, Ann Arbor, MI 48106-1346 USA
313/761-4700 800/521-0600

Order Number 1352942

**Performance effects of a large radome mounted atop a 747-200
aircraft**

Holcomb, Steven Ray, M.S.

The University of Texas at Arlington, 1993

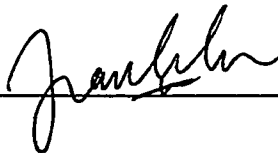
U·M·I

**300 N. Zeeb Rd.
Ann Arbor, MI 48106**

PERFORMANCE EFFECTS OF A LARGE RADOME MOUNTED ATOP A 747-200
AIRCRAFT

The members of the Committee approve the masters
thesis of Steven Ray Holcomb

Frank Lu
Supervising Professor



Don Wilson



Irinel Dragan



PERFORMANCE EFFECTS OF A LARGE RADOME MOUNTED ATOP A 747-200
AIRCRAFT

by
STEVEN RAY HOLCOMB

Presented to the Faculty of the Graduate School of
The University of Texas at Arlington in Partial Fulfillment
of the Requirements
for the Degree of

MASTER OF SCIENCE IN AEROSPACE ENGINEERING

THE UNIVERSITY OF TEXAS AT ARLINGTON

May 1993

ACKNOWLEDGEMENTS

The author would like to thank Wayne Frazier, Mark Hickson and Tim Kelley for their help throughout this program and for their input into this study.

Also, the author would like to thank Dr. Frank Lu for his reading of the draft paper and for his suggestions.

April 6, 1993

ABSTRACT

PERFORMANCE EFFECTS OF A LARGE RADOME MOUNTED ATOP A 747-200 AIRCRAFT

Publication No. _____

Steven Ray Holcomb, M.S.

The University of Texas at Arlington, 1993

Supervising Professor: Frank Lu

The performance characteristics of a 747-200 aircraft, with a large radome mounted atop the fuselage, was analyzed using wind tunnel data. The analysis was based upon six-component force and moment data obtained from low speed and high speed wind tunnel tests of scaled models of the aircraft configurations. The conceptual feasibility of such a configuration was validated by analyzing the aerodynamic loads, performance and stability and control effects.

TABLE OF CONTENTS

ACKNOWLEDGEMENTS.....	iii
ABSTRACT.....	iv
LIST OF FIGURES.....	vi
LIST OF SYMBOLS.....	vii
CHAPTER 1 - INTRODUCTION.....	1
CHAPTER 2 - RADOME SELECTION.....	8
2.1 Radome Shape.....	8
2.2 Radome Incidence Selection.....	9
CHAPTER 3 - RADOME STRUT MODIFICATION.....	10
3.1 Radome Strut Drag.....	10
3.2 Radome Side Force Characteristics.....	13
CHAPTER 4 - CROSS-WIND LANDING.....	15
CHAPTER 5 - TAKEOFF.....	21
CHAPTER 6 - MISSION PROFILE.....	25
CHAPTER 7 - CONCLUSIONS AND RECOMMENDATIONS.....	29
APPENDIX A - PERFORMANCE EQUATIONS.....	31
REFERENCES.....	35

LIST OF FIGURES

Figure 1 : Artist concept of ASTT configuration.....	2
Figure 2 : Texas A&M tunnel installation.....	3
Figure 3 : General arrangement of modification.....	5
Figure 4 : Boeing Transonic Wind Tunnel.....	6
Figure 5 : Four strut configuration; airfoil max t/c 8 per cent; 200 in chord; 35 deg sweep.....	11
Figure 6 : Drag increments of strut configurations....	12
Figure 7 : (a) $\alpha = 3.4$ deg ; (b) $\alpha = 10.1$ deg C_y vs. β for baseline, modified with truss struts, and with 4-strut configuration.....	14
Figure 8 : Airplane landing in a cross-wind.....	16
Figure 9 : C_y vs. β , $M = .25$, in ground effect, 4-Strut, $\alpha = 3$ deg and 10 deg.....	18
Figure 10: Limit cross-wind velocity vs. Approach at $V_A/V_{stall} = 1.3$, Weight = 542990 lb.....	19
Figure 11: Limit cross-wind velocity vs. V_A/V_{stall} approach = 5 deg, Weight = 524990 lb.....	20
Figure 12: Diagram of takeoff BFL sequence.....	22
Figure 13: Engine out BFL vs. center of gravity.....	23
Figure 14: ASTT climb mission profile.....	28

LIST OF SYMBOLS

Coefficients

C_L	= lift/(qS)
C_Y	= side force/(qS)
C_D	= drag/(qS)
$C_{Y\beta}$	= $dC_Y/d\beta$
C_{L_0}	= C_L at zero angle of attack
$C_{L\alpha}$	= Lift curve slope

Angles

δ_c and i_c	= Canard deflection
i_r	= Radome incidence
δ_s and Stab	= Stabilizer deflection
δ_f	= Flap setting
δ_r	= Rudder deflection
α	= Fuselage angle of attack
β	= Sideslip angle
γ	= Angle of flight path to ground
θ	= Approach angle

Constants

b	= Wing span
M	= Mach number
V	= Free-stream velocity
q	= Free-stream dynamic pressure

S	= Wing reference area
FS	= Fuselage station
BL	= Buttline
WL	= Waterline
n_z	= Normal load factor
g	= Gravitational constant

Abbreviations

CG	= Center-of-Gravity
TO	= Takeoff
LDG	= Landing
BFL	= Balanced field length
V_A	= Approach velocity
V_{stall}	= Stall velocity
KCAS	= Knots calibrated airspeed
F_y	= Side force
T	= Thrust
W	= Weight
D	= Drag
L	= Lift
GS	= Ground slope
μ	= Rolling friction
Δt	= change in time
Acc_h	= Horizontal acceleration
Acc_v	= Vertical acceleration

V_h	= Horizontal velocity
V_v	= Vertical velocity
S_h	= Horizontal distance traveled
S_v	= Vertical distance traveled
h	= Height
W_f	= Weight of fuel
TSFC	= Thrust specific fuel consumption
h_{obst}	= Obstacle height
Y	= Side distance

CHAPTER 1

INTRODUCTION

A wind tunnel test program was implemented to validate the conceptual feasibility of installing an elevated radome atop the fuselage of a 747-200 aircraft. The radome will enclose the Advanced Surveillance and Tracking Technology (ASTT) antenna system (Figure 1) and will be mounted 15 feet above the fuselage to meet antenna performance requirements. The validation was accomplished by analyzing the aerodynamic loads, performance, stability and control. Aerodynamic characteristics of the aircraft-radome configuration were obtained from wind tunnel tests of three-percent scaled models. Reported herein are analyses based upon six-component force and moment data obtained from low-speed (Reference 1) and high-speed (Reference 2) wind tunnel tests of the scaled models of the aircraft configurations with and without the radome.

A low-speed wind tunnel test (Figure 2) was conducted at Texas A&M University (Reference 1) to obtain six-component force and moment data on both the unmodified and modified 747-200 models. The modification included a large radome mounted on top of the fuselage, horizontal tail endplates, and canards, as

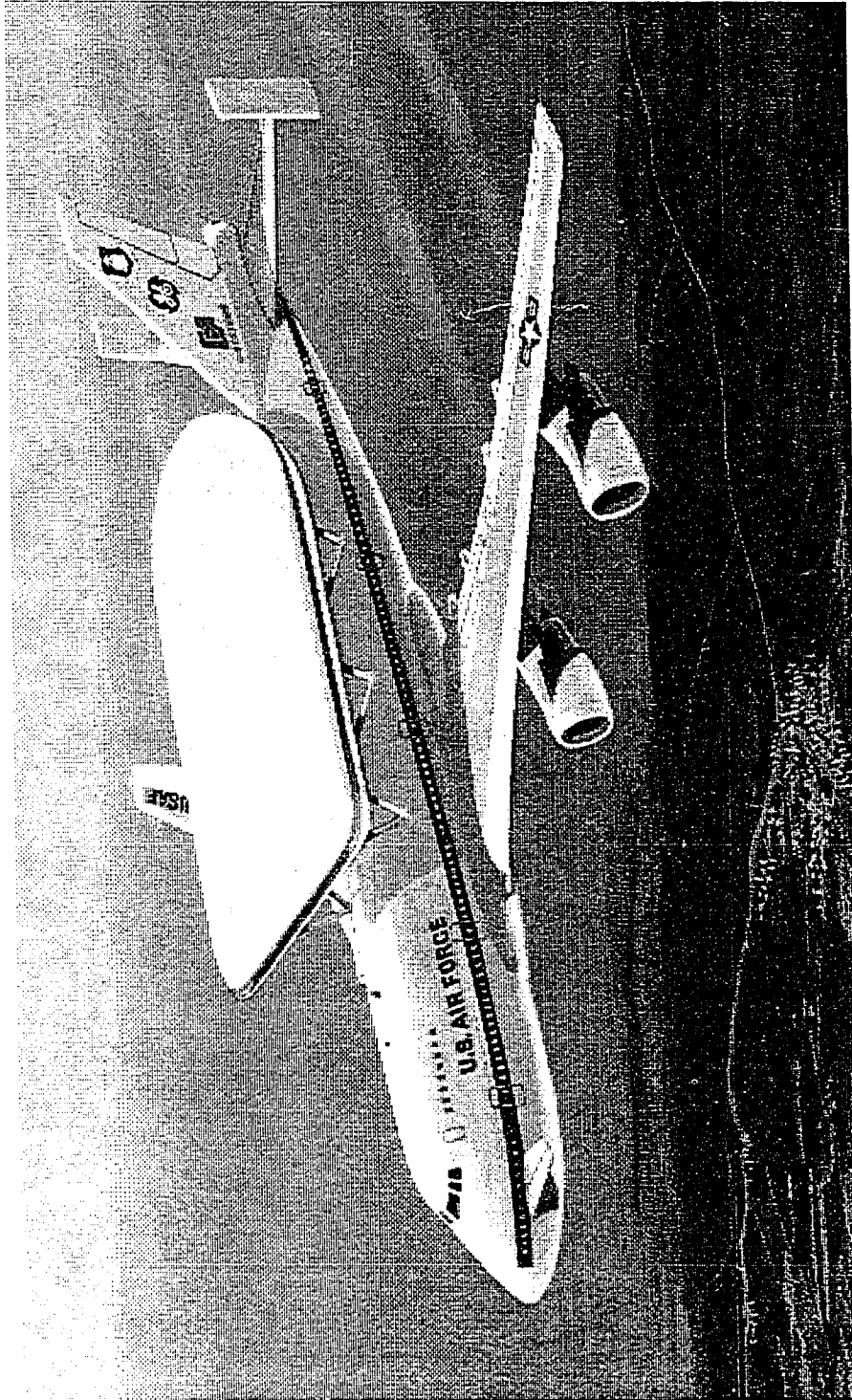


Figure 1: Artist concept of ASTT configuration.

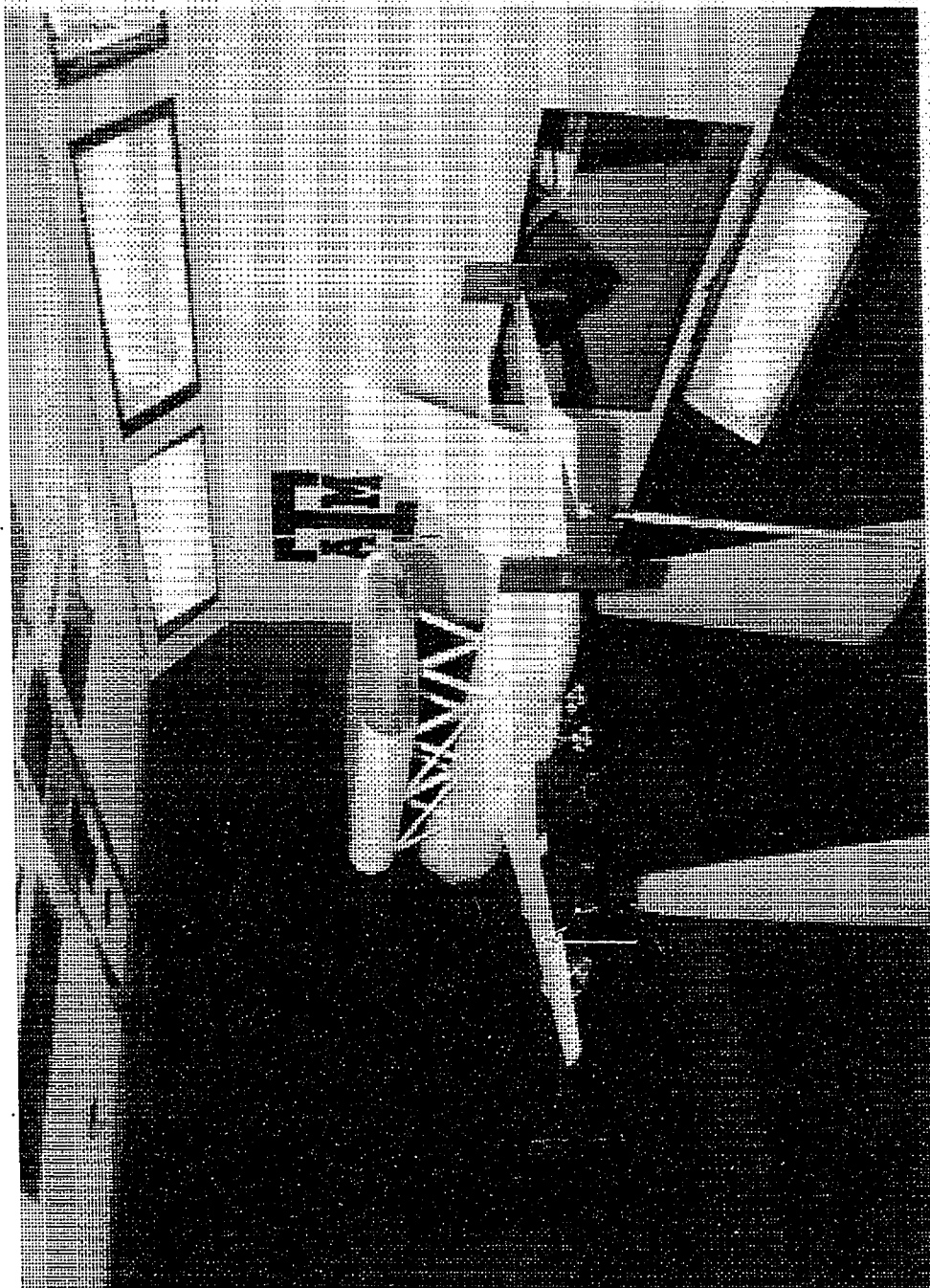


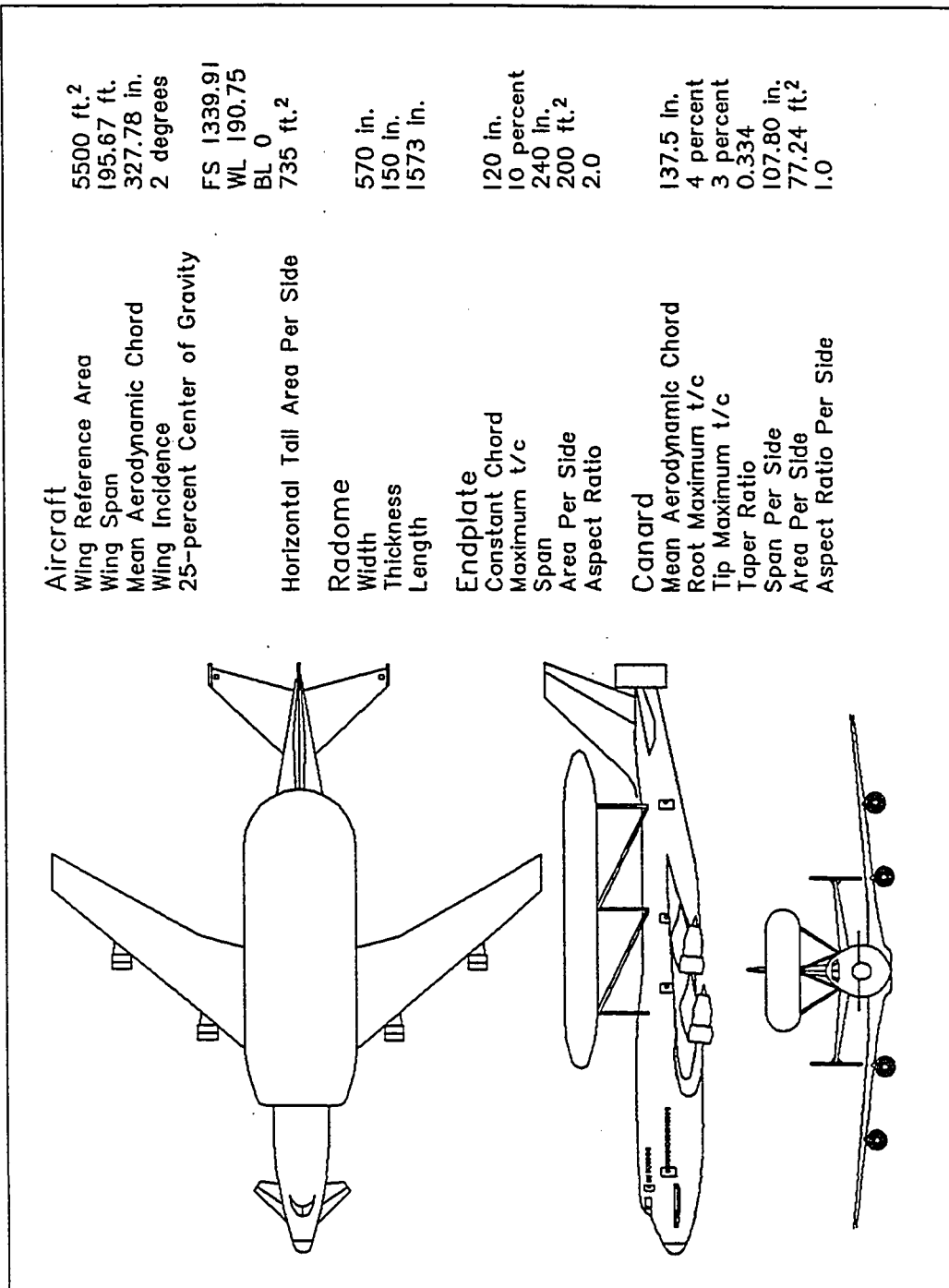
Figure 2: Texas A&M tunnel installation, Reference 1.

shown in Figure 3.

Two different radome fineness ratios of 9.49 and 10.49 were investigated during the test. Takeoff and landing configurations tested included ailerons, spoilers, speed brakes, elevators, horizontal stabilizer, landing gears, rudder and ground effects. Flaps-up testing was conducted for correlating with the high speed wind tunnel results. The low-speed test was to determine the incremental effects of the modifications on the 747-200 aircraft takeoff and landing performance, and stability and control characteristics.

A high-speed wind tunnel test (Figure 4) was conducted at the Boeing Transonic Wind Tunnel (Reference 2) to obtain aerodynamic six-component force and moment data on both the unmodified and modified 747-200 aircraft models. The effects of radome fineness ratios and incidence settings, as for the low-speed test, were investigated during this test. The cruise configuration was tested, including deflection of ailerons, spoilers, speedbrakes, elevators, horizontal stabilizer and rudder. In addition to determining the incremental effects of the modification on performance, stability and control, loads data was collected. The radome was instrumented with a separate balance and pressure taps to obtain independent aerodynamic loads data.

This paper presents the results of a performance analysis of a 747-200 aircraft modified to carry a large radome mounted



SH-03 (ACAD)

Figure 3. General Arrangement of 747-200 with Radome Configurations.

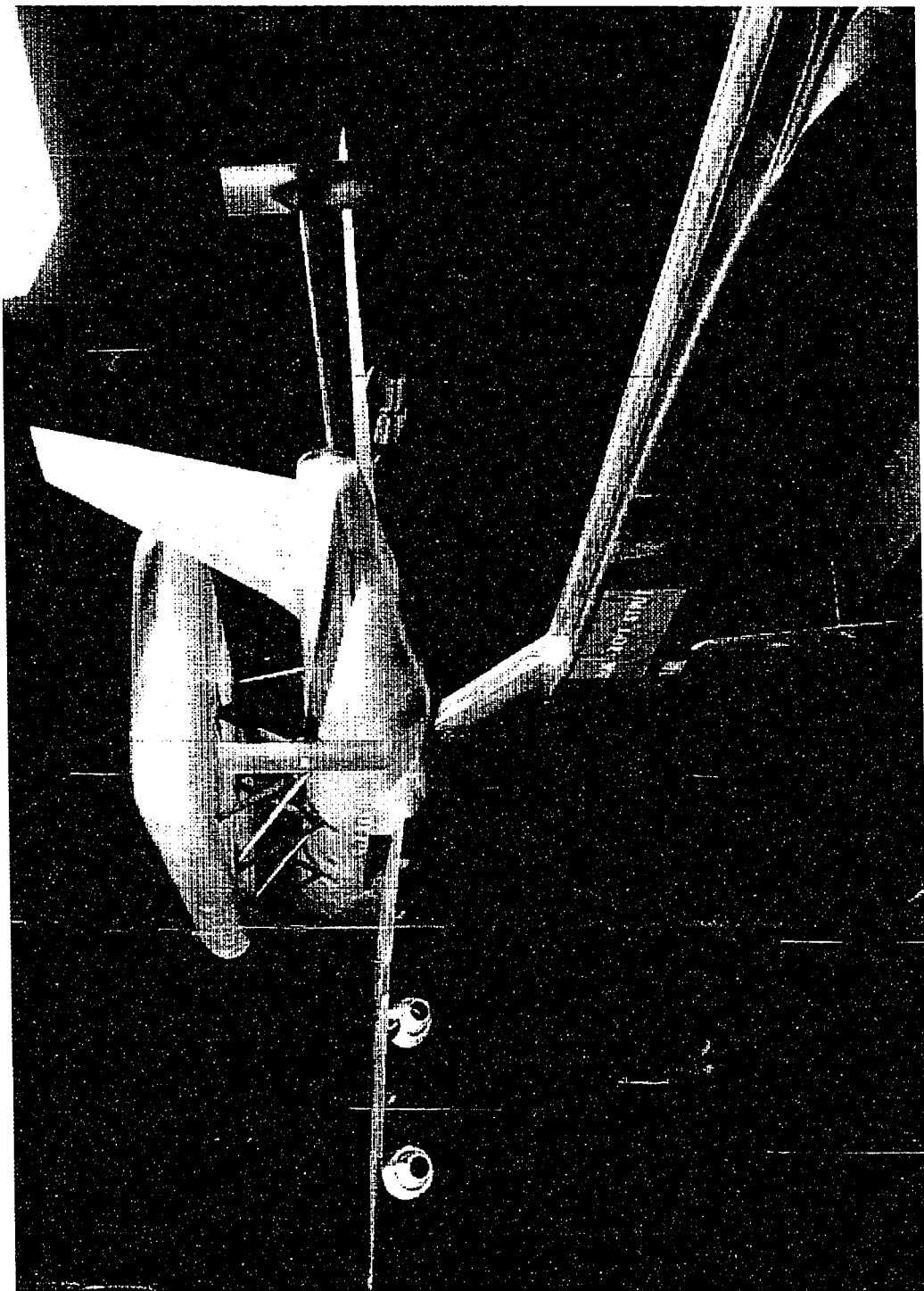


Figure 4: Boeing Transonic Wind Tunnel, Reference 2.

atop the fuselage. The radome incidence and fineness ratio were investigated (Reference 3). The mission performance of the modified aircraft, including takeoff, landing and cruise was investigated.

CHAPTER 2

RADOME SELECTION

2.1 Radome Shape

Of particular concern is the effect of a large radome on the aircraft static and dynamic stability. Thus, a study to select a radome design was performed. Several criteria were used for the selection of the fineness ratio of the radome. The most important criterion was the drag. Secondly, the static longitudinal stability and directional stability were considered. Changes to the lift due to the different configurations were also considered. Radome pressures were used as criteria for determining the fineness ratio. These criteria were analyzed for both the short leading edge/trailing edge configuration and the long leading edge/trailing edge configuration. The fineness ratio chosen was the best configuration based on the above considerations.

The long radome was chosen over the short radome. The aerodynamic characteristics which led to the selection of the long radome over the short radome were examined in detail in Reference 3.

2.2 Radome Incidence Selection

Once the radome configuration was finalized, the radome incidence needed to be selected. The radome incidence was selected by testing the chosen fineness ratio at incidences of 0 deg and -3 deg. The radome fineness ratio was selected by testing two fineness ratios at a radome incidence of 0 deg. The incidences were chosen based on radar platform viewing angle requirements and aircraft configuration performance requirements.

Several criteria were considered when judging which radome incidence to choose. In order of importance, the criteria used were the coefficient of drag, pitching moment, lift, yawing moment, vertical and horizontal tail root bending moment and radome static pressures. For the vertical tail, both static bending moment and RMS values of the dynamic bending moment were used. For the horizontal tail, static bending moment was used. Pressures were collected chordwise on the leading and trailing edges of the radome at the centerline. The -3 deg incidence was selected. Reference 3 examines the data which led to the selection of the -3 deg incidence.

CHAPTER 3

RADOME STRUT MODIFICATION

3.1 Radome Strut Drag

The truss strut configuration (shown in Figures 2 and 4) had incremental drag coefficients of 0.03 to 0.05 at Mach numbers up to 0.70. To reduce the strut drag increment, several configurations were evaluated from empirical methods for drag estimates (Reference 4 and 5). Instead of a large number of small, relatively thick struts, configurations of single, dual and quad struts were conceived. Of these configurations, the four strut arrangement shown in Figure 5 was selected as a feasible alternate to the truss strut configuration shown in Figures 2 and 4.

All of the strut configurations considered had some features in common. The struts had airfoil cross sections with a maximum t/c ratio of 8 per cent. Strut leading edges were swept from 20 deg to 35 deg. Strut planform taper ratios ranged from 1/3 to 1.0. Installed incremental drag of the struts was estimated for five configurations with variations in number of struts and in strut planform parameters (Figure 6). Of the configurations evaluated, the selected configuration satisfied aerodynamic and structural requirements. The single and dual

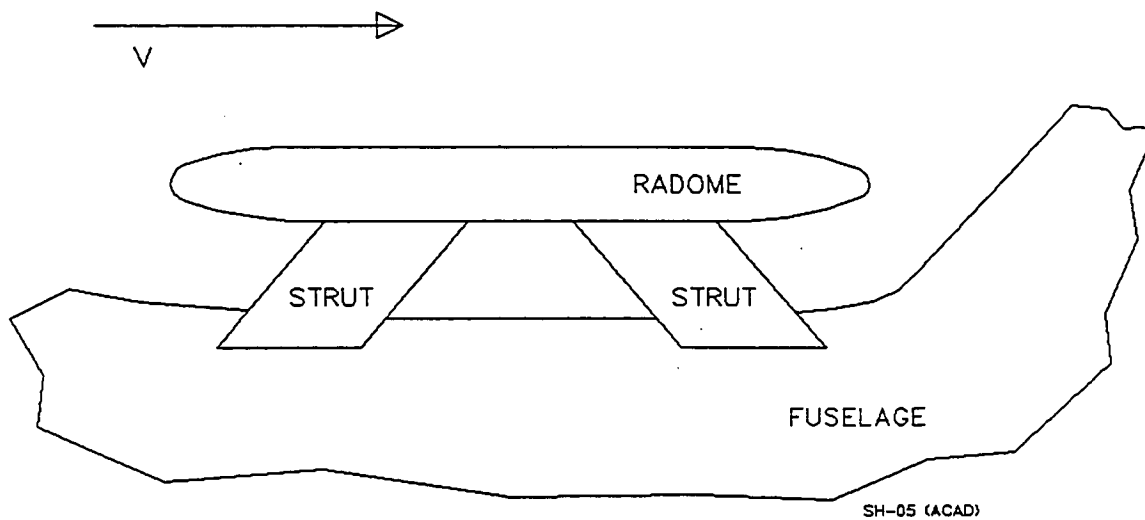


Figure 5. Airfoil Strut Configurations: Four Struts; Airfoil Cross-Section; Maximum Thickness Ratio: 8%; Chord: 200 ins.; Sweep: 35°.

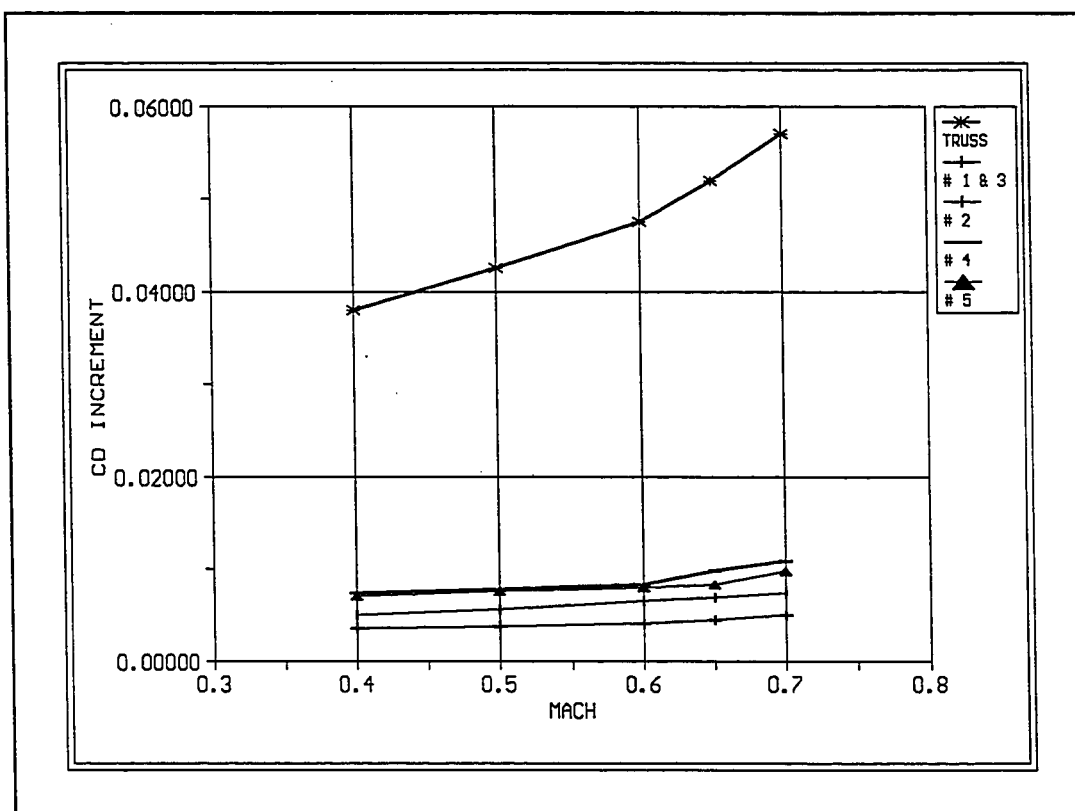


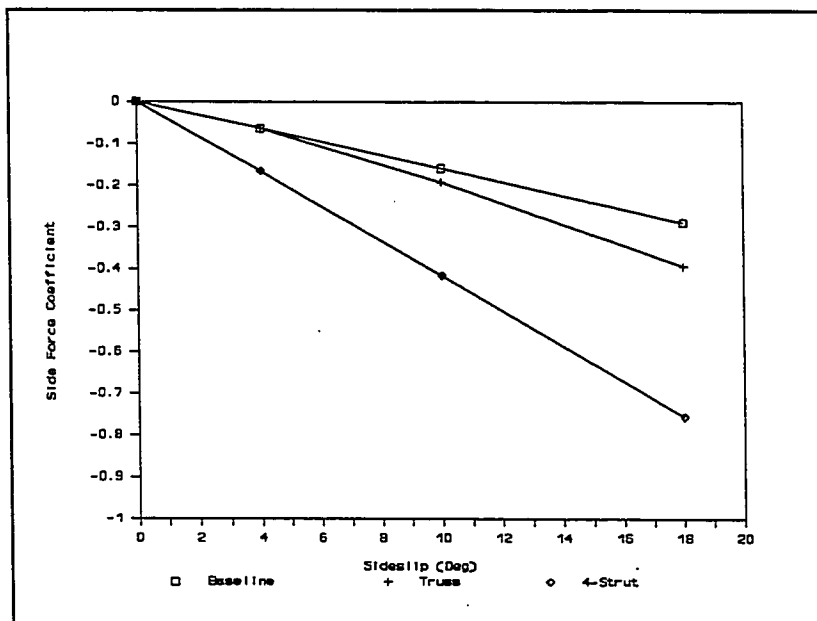
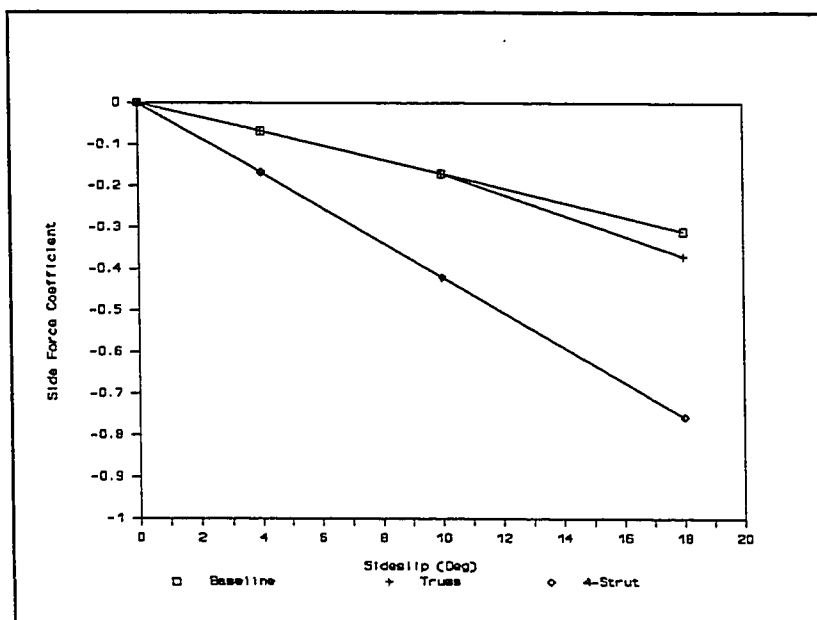
Figure 6: Drag increments of strut configurations.

configurations were eliminated by structural considerations.

3.2 Radome Strut Side-Force Characteristics

Variation of aerodynamic side force with sideslip angle of the four-strut configuration was estimated by treating the four struts as lifting surfaces end-plated at each end. A lift-curve slope of $2\pi/\text{rad}$ or $0.11/\text{deg}$ was assumed for the surfaces. In terms of aircraft reference area the incremental side-force coefficient derivative $\Delta C_{y\beta}$ was $-0.00609/\text{deg}$ per strut. Assuming all four struts were effective in producing side force, the incremental side-force derivative $\Delta C_{y\beta}$ for four struts was $-0.02436/\text{deg}$.

Comparisons of C_y of the baseline aircraft and of the modified aircraft with truss struts and with 4-struts, are shown in Figures 7a and 7b for angles of attack of 3.4° and 10.1° , respectively, at $M = 0.4$. Variation of C_y with β at both angles of attack for the modified aircraft, with the truss strut configuration, exhibited some non linearity with increasing β , especially above 10° . C_y for the truss struts was 20 per cent greater than the baseline aircraft at 3.4° angle of attack. C_y of the modified aircraft with the four-strut configuration is estimated to be 1.6 times that of the baseline aircraft at $\alpha = 3.4^\circ$ and $\beta = -10^\circ$.

(a) $\alpha = 3.4$ deg(b) $\alpha = 10.1$ degFigure 7: C_y vs. β for baseline, truss struts, and 4-strut.

CHAPTER 4

CROSS WIND LANDING

The cross-wind velocity limit was based on the side translation of the aircraft not exceeding 75 feet. The side translation limit of 75 feet was chosen since by lining up on the centerline of a narrow runway, 150 feet wide, the pilot would have 75 feet in which to translate. This is conservative since lining up the aircraft upwind of the runway centerline would allow more runway width for translation. Lift, drag, and side-force characteristics from the wind tunnel data base were used to define the input parameters to calculate the landing characteristics of the modified aircraft. Two different strut configurations were used to calculate the side translation of the modified aircraft. The first strut configuration analyzed was the original truss configuration tested in the wind tunnel. The second strut configuration analyzed was the four-strut configuration, designed to have less drag than the original configuration. The second strut configuration produced a higher side force; therefore, the side translation increased.

Figure 8 shows the modified airplane landing under a cross-wind condition. The side translation was calculated from barrier clearance (50 feet height), with the nose lined up to

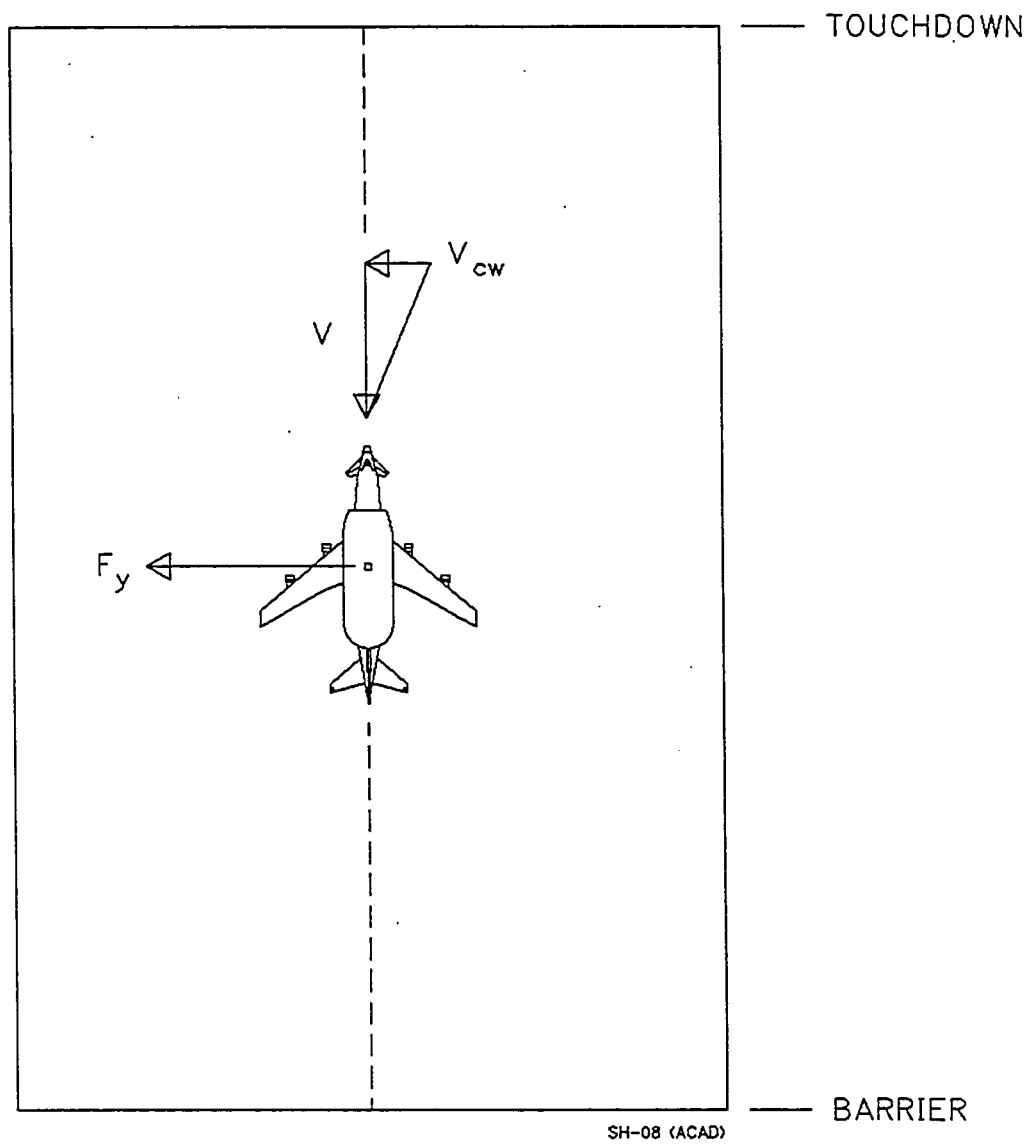


Figure 8. The Modified Airplane Landing Under a Cross-wind Condition.

the centerline, to aircraft stop. The pilot could crab the aircraft longer to take out the side force, but the barrier was chosen as a conservative point to straighten the airplane with the runway. Side-force coefficient variation with sideslip for the new strut configuration is shown in Figure 9 ($\alpha = 3$ deg and 10 deg). See Appendix A for equations.

The limit cross-wind velocity for the new and old strut configurations are 6 and 13 knots, respectively. As can be seen from Figure 10, the cross-wind landing capability of the new strut configuration is unsatisfactory for an angle of approach of 3 deg and an approach velocity of $1.3V_{stall}$. The approach angle was optimized for cross-wind landing capability. Figure 10 indicates that the optimum approach angle is 5 deg. With a 20 knot increase of the approach velocity, V_A/V_{stall} became 1.5, as opposed to 1.3. Figure 11 shows the cross-wind velocity limit plotted against V_A/V_{stall} . From Figure 11 the cross-wind limit velocity at $V_A/V_{stall} = 1.5$ is 15 knots.

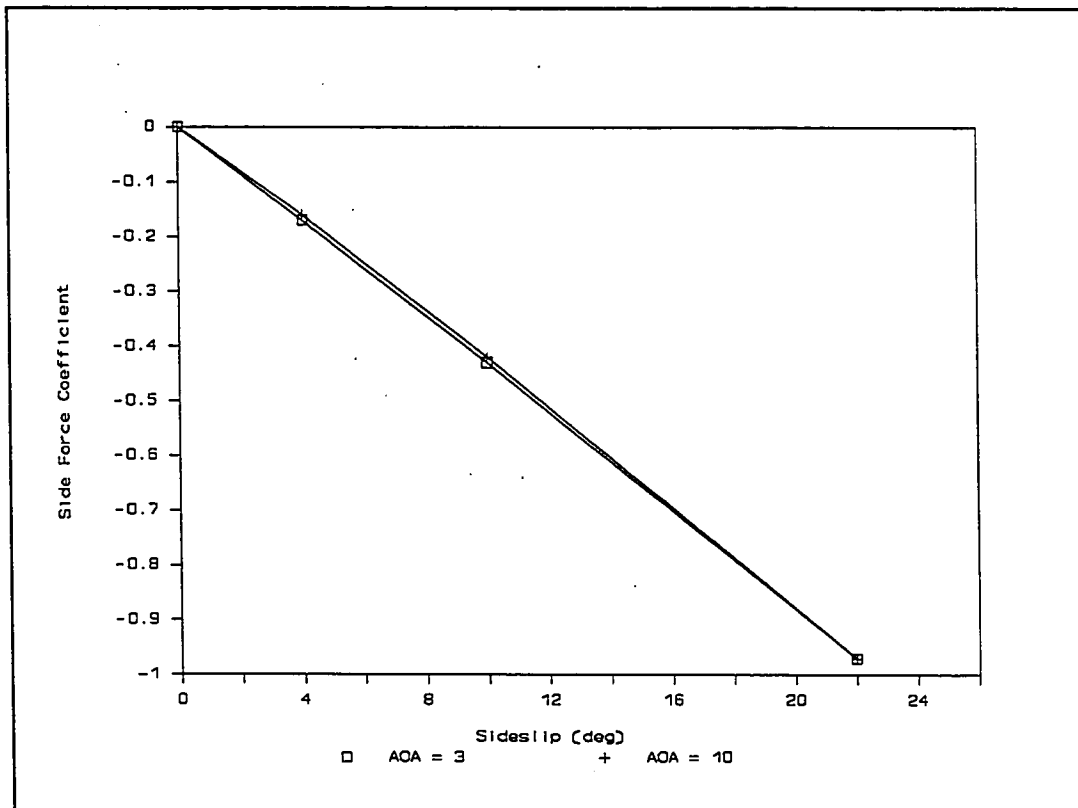


Figure 9: C_y vs. β , $M = 0.25$, in ground effect, 4-Strut, $\alpha = 3$ deg and 10 deg.

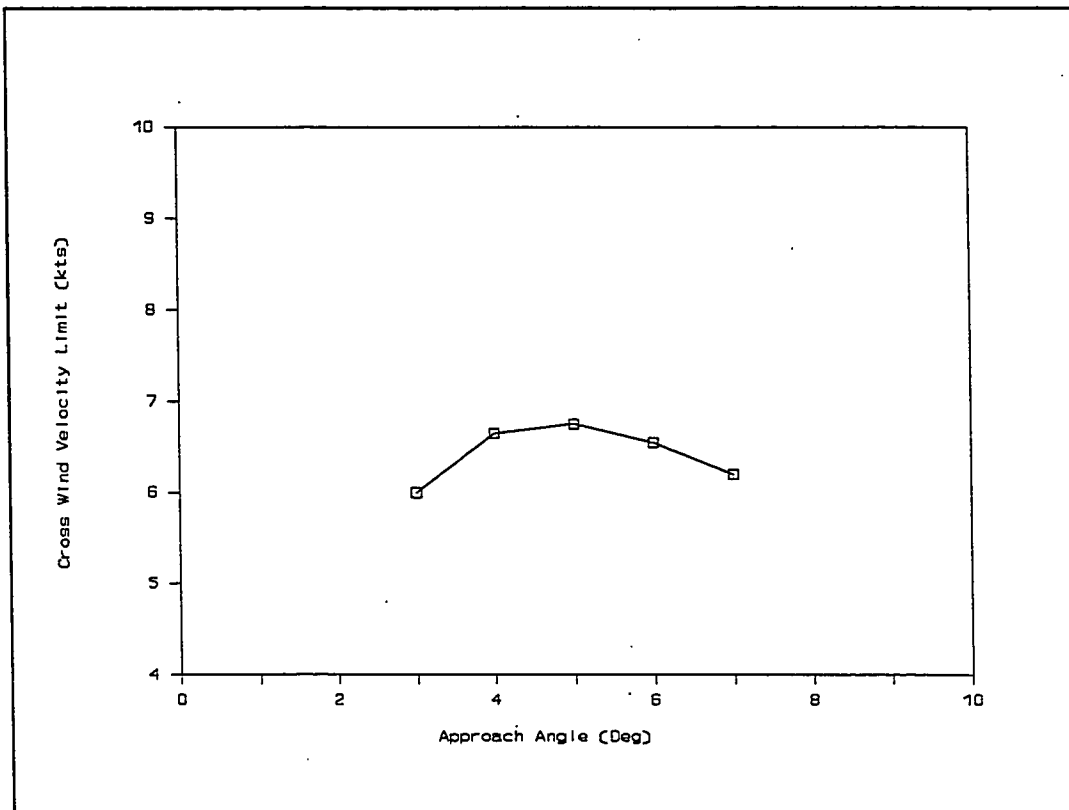


Figure 10: Limit cross-wind velocity vs. Approach angle; at $V_A/V_{\text{stall}} = 1.3$, Weight = 542,990 lb.

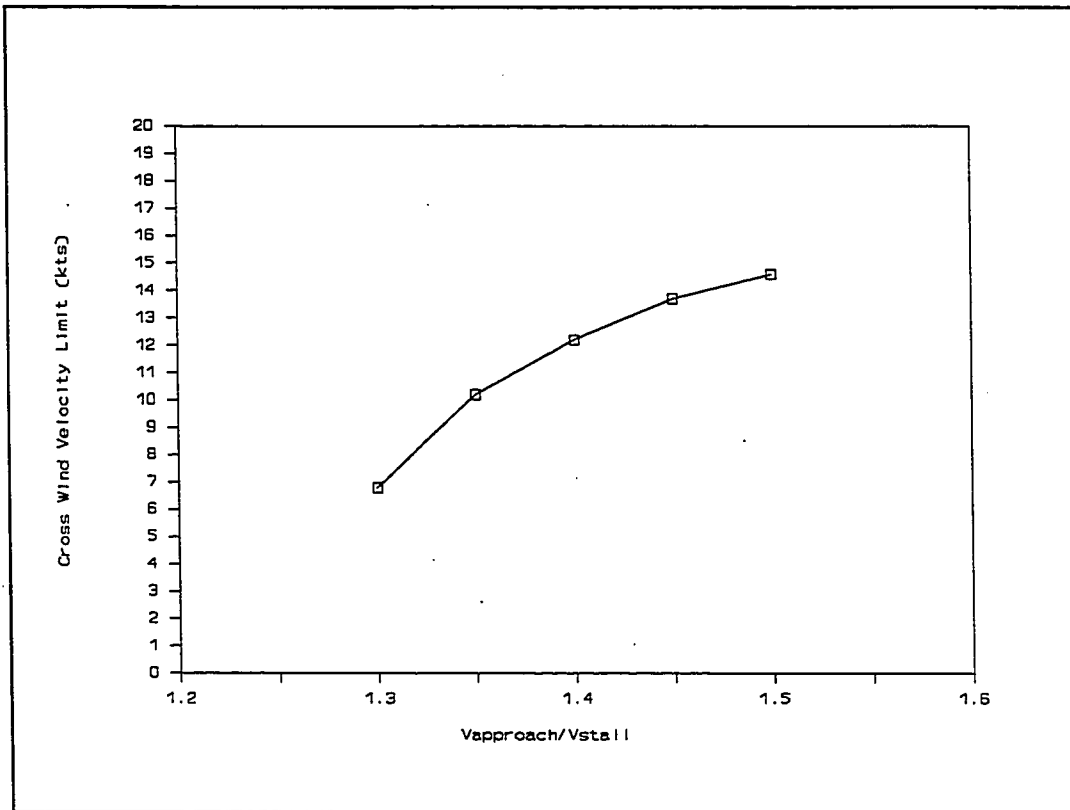


Figure 11: Limit cross-wind velocity vs. V_A/V_{stall} at Approach angle = 5 deg, Weight = 524,990 lb.

CHAPTER 5

TAKEOFF

The balanced field length calculation is needed to determine if the aircraft can takeoff from a specified airfield safely. The balanced field length calculation is the length where, with an engine failure, the aircraft can either takeoff or stop in the same distance. Figure 12 shows a diagram of the balanced field length. The aircraft is accelerated with four engines until one of the engines fails. Then, there is a small delay before the pilot makes his decision to takeoff or stop. For the takeoff decision, the rotation is initiated, then liftoff occurs. The next segment is the takeoff climb to 35 feet.

The balanced field length calculations were performed at various weights and center of gravity locations. The maximum takeoff weight of the modified aircraft is 800,000 pounds with a center of gravity location of 20.5 per cent. Figure 13 contains the balanced field length variation with center of gravity for a series of takeoff weights. From this figure it can be seen that for a takeoff gross weight of 800,000 lbs and a center of gravity of 20.5 per cent MAC, the balanced field length is approximately 11,500 feet. From Figure 13, the

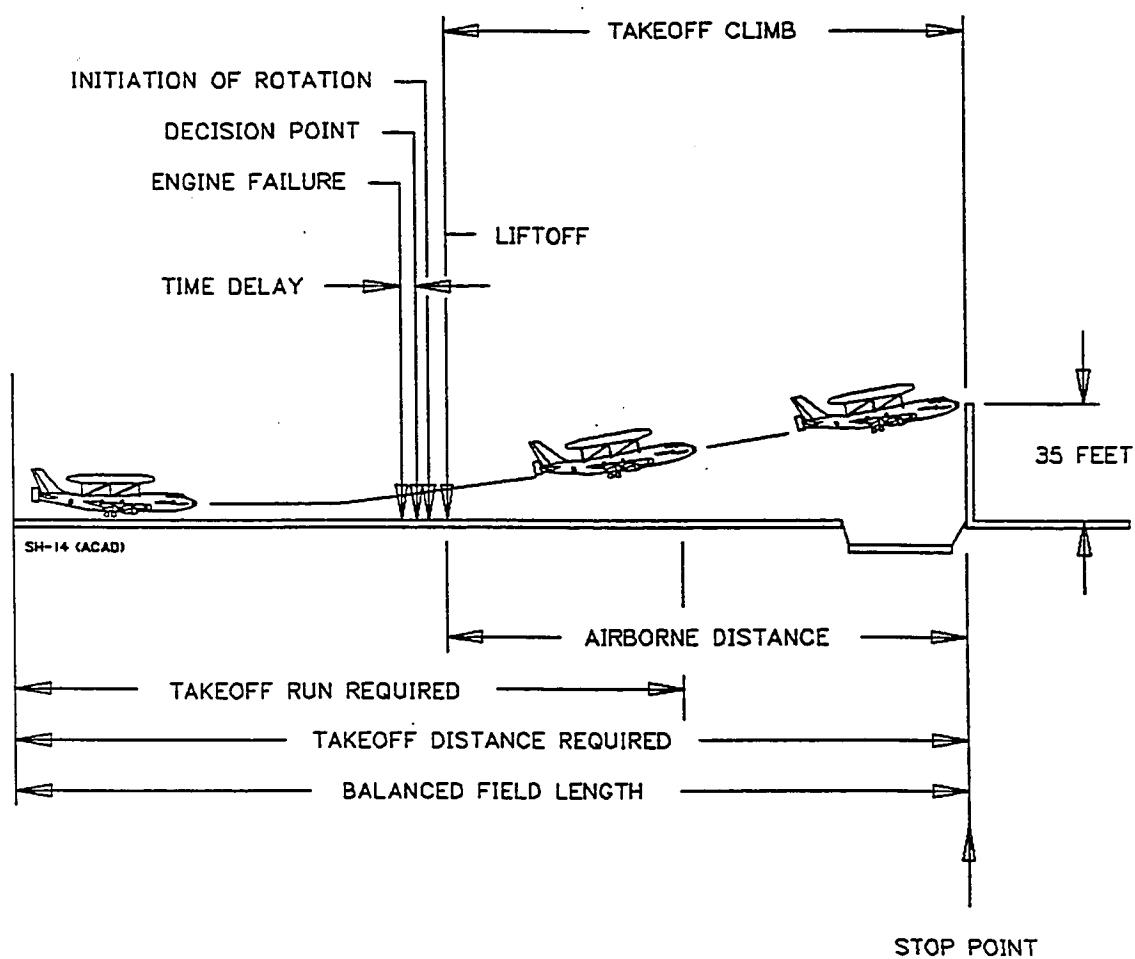


Figure 12. Diagram of the Takeoff Balanced Field Length Sequence.

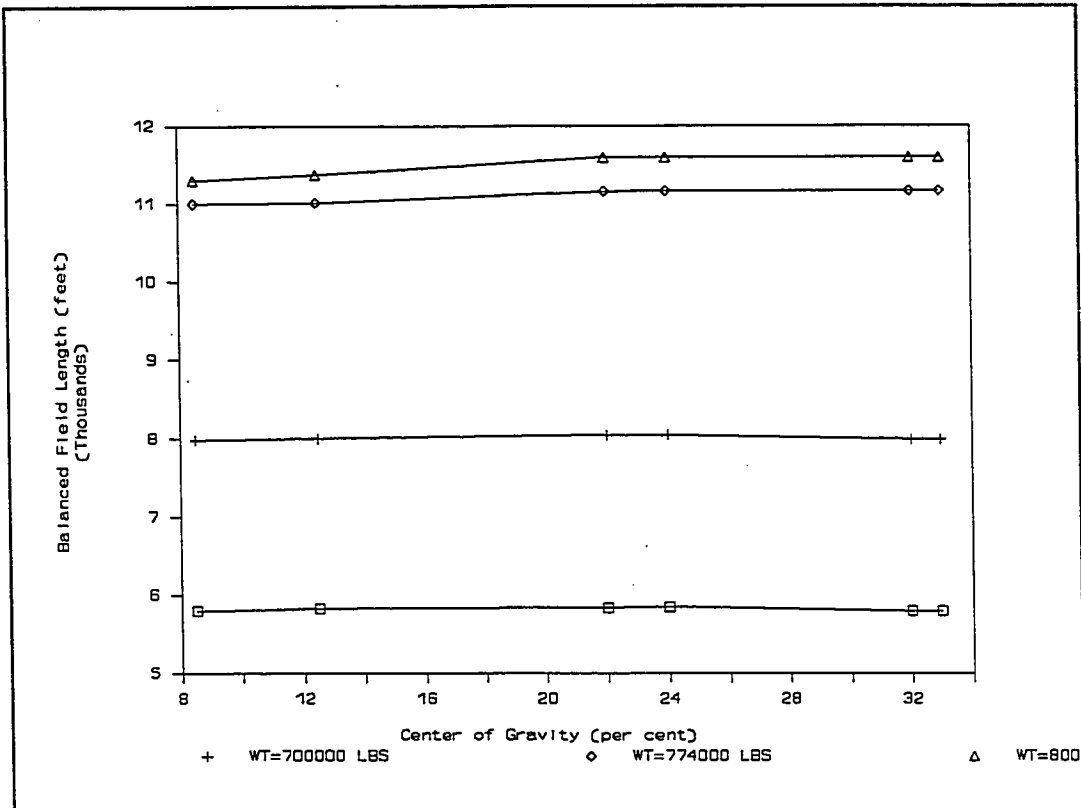


Figure 13: Engine out BFL vs. Center of Gravity.

balanced field length can be interpolated for various weights and allowable center of gravity locations. See Appendix A for equations.

CHAPTER 6

MISSION PROFILE

The trimmed lift coefficient values, including canard and stabilizer, were obtained from a computer program (Appendix A) which utilized wind tunnel data from the high and low speed wind tunnel tests. Trimmed lift coefficient values were obtained for maximum lift-to-drag ratio (L/D) and minimum drag cases.

Trimmed drag coefficient values (C_D) were also obtained from the aforementioned program. Again, trimmed drag coefficients were obtained for maximum L/D and minimum C_D cases. The maximum L/D calculated for various Mach numbers were found to lie on the corresponding minimum C_D curves also obtained at those values of Mach number.

The thrust available and corresponding fuel-flow rates were obtained from available information on the CF6-50E engine used for the Boeing 747 aircraft. This information was used for the modified aircraft to determine maximum continuous thrust, takeoff thrust, maximum cruise thrust and idle thrust at various altitudes. Takeoff was determined using takeoff thrust, climb was performed at maximum continuous thrust, range was calculated using both maximum continuous thrust and cruise thrust while descent and approach utilized idle thrust.

The performance analysis allowed fuel usage for takeoff, climb, descent, approach and reserve. A step climb was evaluated in order to achieve maximum altitude and range.

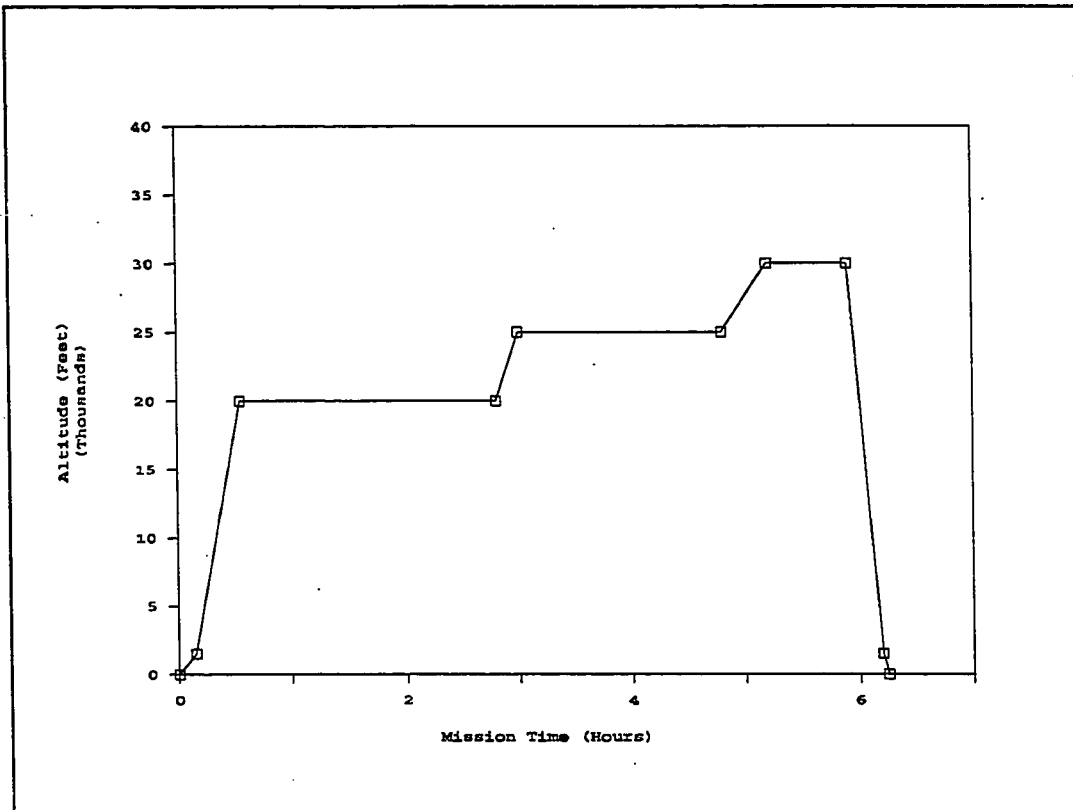
Trimmed maximum L/D was used to calculate the takeoff segment of the mission profile. The takeoff segment was considered to begin at sea level and end at 1,500 feet. The ground roll to takeoff was added to the range for this segment of the mission profile.

The mission profile utilized a step climb to 20,000 feet, 25,000 feet and eventually 30,000 feet, followed by descent and land. This profile was considered to provide more range and time in the air for the aircraft while achieving the maximum altitude possible. The actual climb schedule used to reach each altitude was an enroute climb schedule which consisted of a constant calibrated airspeed climb segment followed by a constant Mach climb segment. The step climb mission profile consisted of a 265 KCAS climb up to 20,000 feet, cruise, then a 255 KCAS climb to 23,000 feet followed by a constant Mach climb segment ($M = 0.6$) to 25,000 feet. After the second cruise segment was completed, a 285 KCAS climb was used to reach an altitude of 30,000 feet. The time and range for each mission during the climb are shown in Figure 14. The climb schedule was determined to maximize rate of climb such that the aircraft reaches the desired altitude (30,000 feet) as heavy as possible. Climb segments were flown in order to maximize L/D. The cruise

segments of each mission profile were simply flown at speeds necessary to achieve best mileage per pound of fuel. The time at altitude for each mission profile is shown in Figure 14. All cruise segments were flown in such a way as to minimize drag.

Descent segments were also flown in order to minimize drag. The descent segments for the mission profile began with a $M = 0.6$ descent down to 15,000 feet followed by a 250 KCAS descent to 1,500 feet. These speeds helped to achieve best nautical mile per pound of fuel for this phase of the mission. The time during this segment is also shown in Figure 14.

The reserve fuel was calculated to be 5 per cent of the total fuel used from the start of the mission through the approach segment. The amount of reserve fuel for each mission is shown in Figure 14.



TOGW	800,000	Lbs
Fuel	262,790	Lbs
Reserve fuel	30,782	Lbs
Time at altitude	2	hours
Range at 20,000 ft	675	NM
Time at altitude	1.9	hours
Range at 25,000 ft	680	NM
Time at altitude	0.7	hours
Range at 30,000 ft	338	NM
Total range	2,220	NM

Figure 14: ASTT climb mission profile.

CHAPTER 7

CONCLUSIONS AND RECOMMENDATIONS

Based on the wind tunnel data and analysis presented in this report, the ASTT design concept is aerodynamically acceptable from a performance viewpoint. The following recommendations are offered. The wind tunnel test data indicated the higher fineness ratio or long radome at the -3 deg incidence is the preferred configuration. The drag for this configuration was significantly less than that of the short radome. There was not much difference in the other criteria between the two radomes or two incidences tested.

All of the mission profile segments were determined by trimming the aircraft with a combination of canard and stabilizer such that maximum L/D or minimum drag was maintained. Due to the decrease in longitudinal stability of the modified aircraft, encountering a gust will require rapid canard response to maintain desired stability. Since the negative incidence response will start from a moderate negative incidence trim setting, at worst case, sufficient canard motion will remain to allow for the immediate response necessary to maintain static-longitudinal stability. Further studies should involve a tailoring of the canard/stabilizer trim combination to

maintain sufficient canard incidence margin for gusts.

At cruise, the radome drag is 100 to 120 counts. The truss-strut configuration tested had a drag of 380 to 750 counts which is unacceptable for performance requirements. The new strut configuration, designed for aerodynamic drag consideration, was determined to have a drag count of 70 to 100 at cruise speeds.

The potential for minimizing the strut drag (and side force effects) exists in properly tailoring the shape and size of the struts. A step climb profile to 30,000 feet indicates a total range of 2,220 nautical miles and a total mission time of 6.2 hours with a maximum takeoff gross weight of 800,000 lbs. With a one-engine-out failure, the balanced field length of the modified aircraft is 11,700 feet based on the maximum takeoff gross weight. The cross-wind landing capability of the modified aircraft is a maximum 15 knot cross-wind velocity.

APPENDIX A
PERFORMANCE EQUATIONS

APPENDIX A

A.0 PERFORMANCE EQUATIONS

The performance equations shown below were obtained from Reference 6.

A.1 TAKEOFF EQUATIONS

A computer program was written to calculate the balanced field length of the ASTT aircraft. The balanced field length calculation requires four segments to be determined. The four segments are: 1) ground run, 2) rotation, 3) climb to thirty five feet, and 4) stop distance from engine failure. The aircraft makes a ground run until an engine failure and at that time the aircraft can either continue takeoff or stop. The set of equations for each segment is shown below.

1) GROUND RUN

The ground run calculation was done by calculating the acceleration and incrementing it by .001 seconds until the rotation velocity was met. The equations used are shown below:

$$Acc_h = g * ((T/W) - (D/W) - (\mu * (L/W)) - GS)$$

$$V_i = V_{i-1} + (\Delta t * Acc_h)$$

$$s_h = s_h + (V_{havg}) * \Delta t.$$

2) ROTATION

The rotation to liftoff calculation was performed similar to the ground run. The equations used are shown below:

$$Acc_h = g * ((T/W) - (D/W) - (\mu * (1-L/W)) - GS)$$

$$V_i = V_{i-1} + (\Delta t * Acc_h)$$

$$s_h = s_h + (V_{havg}) * \Delta t.$$

These equations were used until the lift became higher than the weight and then liftoff occurs.

3) CLIMB TO THIRTY FIVE FEET

$$Acc_h = (g / (W * n_z)) * (T * \cos(\alpha) - D(W * n_z * \sin(\gamma)))$$

$$Acc_v = (g / W * n_z) * (L - (W * n_z * \cos(\gamma)) + (T * \sin(\alpha)))$$

$$V_{hi} = V_{hi-1} + (\Delta t * acc_h)$$

$$V_{vi} = V_{vi-1} + (\Delta t * acc_v)$$

$$S_h = S_h + (V_{havg} * \Delta t)$$

$$h_i = h_{i-1} + (V_{vavg} * \Delta t)$$

Climb until height is thirty five feet.

4) STOP DISTANCE FROM ENGINE FAILURE

$$Acc_h = (g/W) * (T-D - (\mu * (1-L)) - GS)$$

$$V_{hi} = V_{hi-1} + (\Delta t * acc_h)$$

$$S_h = S_h + (V_{havg} * \Delta t)$$

A.2 CLIMB EQUATIONS

The climb calculations were made with an incremental time stepping routine. The equations used are shown below:

$$R/C = V * (T-D) / W$$

$$h_i = h_{i-1} + (V * \sin(\gamma) * \Delta t)$$

$$Range_i = Range_{i-1} + (V * \cos(\gamma) * \Delta t)$$

A.3 RANGE EQUATIONS

The range calculations were made using an incremental time for stepping through each altitude. The equations used for calculating the range at a certain condition are shown below:

$$T = D$$

$$W_f = T * TSFC * \Delta t$$

$$Range_i = Range_{i-1} + (V_t * \Delta t)$$

A.4 LANDING EQUATIONS

A computer program was written to calculate the landing distance of the ASTT aircraft. Also, the side translation of the aircraft in a crosswind landing is calculated. The landing distance calculation requires four segments to be determined. The four segments are: 1) approach, 2) flare, 3) transition, and 4) ground roll to stop.

1) APPROACH

The approach calculation was done by setting the approach velocity and calculating approach angle such that the vertical acceleration was less than 10 ft/sec². Thus knowing the obstacle height and having solved for the optimum approach angle the time and distance traveled could be calculated. The equations used are shown below:

$$Acc_v = g * (W * \sin(\theta) - D)$$

$$s_h = h_{\text{obst}} / \tan(\theta).$$

2) FLARE

The flare equations are shown below:

$$C_{L\text{flare}} = C_{L0} + (C_{L\alpha} * \theta_{\text{flare}})$$

$$n_z = C_{\text{flare}} / C_{L\text{approach}}$$

$$s2 = (V_A^2 * \tan(\theta)) / (2 * g * (n_z - 1))$$

$$t2 = s2 / V_A.$$

$$Y2 = (F_y / W) * g * t^2 * .5$$

3) TRANSITION

$$Acc_h = (((T - D) / W) - (\mu * (1 - L / W))) * g$$

$$V_i = V_{i-1} + (\Delta t * acc_h)$$

$$s3 = s3 + (V_{\text{avg}} * \Delta t)$$

$$t3 = t3 + \Delta t$$

$$Y3 = (F_y / W) * g * t3^2 * .5$$

4) GROUND ROLL TO STOP

$$Acc_h = (g / W) * (T - D - (\mu * (1 - L)) - GS)$$

$$V_i = V_{i-1} + (\Delta t * Acc)$$

$$S4 = S4 + (V_{\text{avg}} * \Delta t)$$

REFERENCES

1. Boeing Staff: "Boeing Transonic Wind Tunnel Test 2100", BTS-T-1851-1A Volume 1-4. December 1990, Seattle, WA.
2. Steen, Greg: "Three Per Cent Scale Model of 747-200 with Radome Test Report", Technical Report No. 9029. Texas A&M Wind Tunnel, November 1990, College Station, TX.
3. Frazier, W. E.: "Longitudinal and Directional Static Stability Effects of a Large Radome Mounted Atop a 747-200 Aircraft" AIAA-91-3173, AIAA Aircraft Design Systems and Operations Meeting, September 23-25, 1991, Baltimore, MD.
4. Hoerner, S.F.: Fluid Dynamic Drag published by author. NJ, 1958.
5. Anonymous: USAF Stability and Control Datcom. AF33(616)-6460 Air Force Flight Dynamics Laboratory, Wright-Patterson Air Force Base, October 1960 (rev. August 1968).
6. McCormick, B.W.: Aerodynamics, Aeronautics, and Flight Mechanics published by Wiley and Sons, New York, 1979.

